Phyton-
International Journal of
Experimental Botany

Tech Science Press

http://doi.org/10.32604/phyton.2026.078590

ARTICLE

Integrated Transcriptome and Lipidome to Analyze the Characteristics of Oil Accumulation in Seeds of *Acer truncatum*

Shengqun Chen[1,2,#], Lianwen Shen[1,2,#], Shuang Qu[1,2], Xia Jiang[1,2,3,*] and Gang Wang[1,2,4,*]

[1]Key Laboratory of National Forestry and Grassland Administration on Biodiversity Conservation in Karst Mountainous Areas of Southwestern China, Guizhou Academy of Forestry, Guiyang, China
[2]Guizhou Academy of Forestry, Guiyang, China
[3]Guizhou Liping Rocky Desertification Ecosystem Observation and Research Station, Qiandongnan Prefecture, China
[4]Qianxing Agricultural and Forestry Economic Development Co., Ltd., Liuzhi Special Zone, Liupanshui, China
*Corresponding Authors: Xia Jiang. Email: jingle2411@163.com; Gang Wang. Email: wang3540307@163.com
#These authors contributed equally to this work

Received: 04 January 2026; Accepted: 05 March 2026; Published: 28 April 2026

ABSTRACT: *Acer truncatum* is a significant woody oil-bearing tree species known for its ability to synthesize various unsaturated fatty acids. This study systematically analyzes the lipid metabolic pathways and the associated transcript abundance changes involved in the biosynthesis and accumulation of seed oil in *A. truncatum*. By integrating lipidomics and transcriptomics analyses across different developmental stages of *A. truncatum* seeds, we thoroughly investigate the dynamic characteristics of oil metabolism. The results show that triacylglycerols (TAGs) become the dominating lipid class throughout seed development and that their amount increases greatly as the seeds mature, whereas diacylglycerols (DAGs) show a significantly decreased relative abundance. Numerous differentially expressed genes (DEGs) linked to lipid biosynthesis were identified by transcriptome analysis, including *AcACCase*, *AcKAS*, *AcKCS*, *AcGPAT*, *AcDGAT*, and *AcOLE*. The expression patterns of DGAT- and KCS-encoding genes differ noticeably between immature and mature seeds. Integrated lipidomics and transcriptomics analyses suggest stage-associated lipid metabolic changes during seed development of *A. truncatum*. This study also highlights candidate genes and metabolic pathways with TAG accumulation. These findings improve our understanding of seed oil metabolism in *A. truncatum* by linking *Ac*DGAT-related TAG assembly and *Ac*KCS-driven very-long-chain fatty acid elongation to the developmental regulation of the Kennedy pathway (TAG biosynthesis) and fatty acid elongation (VLCFA/NA-related), providing essential molecular insights for the genetic improvement of oil yield and fatty acid quality in this species.

KEYWORDS: *Acer truncatum*; triacylglycerols; diacylglycerols; *DGAT*; *KCS*

1 Introduction

Acer truncatum Bunge is a deciduous maple tree that is native to northern China, Japan, and Korea, and has since been introduced to Europe and North America [1,2]. Compared to common edible seed oils such as sunflower, rapeseed, and peanut oils, the oil derived from this species contains an exceptionally high proportion of unsaturated fatty acids, particularly linoleic acid (LA) and oleic acid (OA), whose concentrations can even surpass those found in these conventional oils [3,4]. The seed oil is distinguished by a high proportion of unsaturated fatty acids, particularly linoleic acid (LA) and oleic acid (OA), with levels that can surpass those found in conventional seed oils such as sunflower, rapeseed, and peanut [5], *A. truncatum* seed oil contains about 5–6% nervonic acid (NA), a very-long-chain monounsaturated fatty acid

Copyright © 2026 The Authors. Published by Tech Science Press. This work is licensed under a Creative Commons Attribution 4.0 International License, which permits unrestricted use, distribution, and reproduction in any medium, provided the original work is properly cited.

originally described from mammalian nervous tissue. Nervonic acid has been implicated in the development and maintenance of the nervous system and in the biosynthesis of neuronal cell membranes [1,6,7]. Notably, besides *A. truncatum*, NA is also found in other plants, such as *Lunaria annua*, *Tropaeolum speciosum* [8], and *Ankyropetalum* [9]. Among these species, although the seed oil of *A. truncatum* contains only 5–6% NA, its high fruit yield and the ease of seed oil production contribute to a substantial output of NA [10]. In 2011, the National Health Commission of the People's Republic of China officially approved the seed oil of *A. truncatum* as a new resource for edible oil. However, this species remains underutilized as a nutraceutical oil tree, and its potential—particularly regarding lipid accumulation and regulation—has yet to be fully explored [11].

In most higher plants, storage oil, primarily composed of triacylglycerols (TAGs), serves as the primary carbon and energy reserve for seed germination. TAGs consist of three long-chain fatty acids (FAs) esterified to a glycerol backbone. TAGs are the most energy-dense type of stored lipids found in eukaryotic cells [12]. The FA composition of seed TAGs significantly influences the physicochemical properties of the oil, thereby determining its suitability for nutritional use, industrial feedstocks, or biofuel production [13–15]. In plants, *de novo* FA synthesis occurs in plastids, after which the acyl chains are incorporated into TAG either through the acyl-CoA-dependent Kennedy pathway or via the phospholipid: diacylglycerol acyltransferase (PDAT) pathway, which transfers acyl groups from membrane phospholipids [16–18]. Both pathways typically operate in parallel, contributing to TAG pools with distinct FA compositions [14,18,19]. Although the core reactions of *de novo* lipid biosynthesis are well characterized, the relative metabolic flux directed toward diacylglycerol (DAG) and TAG synthesis varies among species, developmental stages, and environmental conditions, resulting in diverse TAG molecular species and ultimately influencing seed oil composition [13,20]. The final acylation reaction, which converts diacylglycerol (DAG) into triacylglycerol (TAG), is catalyzed by acyl-CoA:diacylglycerol acyltransferase (DGAT) [18]. This reaction represents a critical control point for lipid accumulation in developing oilseeds [19,21]. Thus, clarifying how the DAG and TAG biosynthetic pathways are coordinated is essential for understanding seed oil formation and for rationally engineering high-quality edible oils in *A. truncatum*.

Despite earlier studies focusing on the fatty acid composition and seed oil content of *A. truncatum* [1,22], as well as its regional and genotypic variations [23,24], limited information is available regarding the regulatory mechanisms governing TAG and DAG production and accumulation through lipidomic and transcriptomic analyses [10]. The relationship between lipidomic metabolite changes during seed maturation and the associated metabolic pathways remains largely unknown [6,25]. In this investigation, comparative lipidomic and transcriptome analyses were conducted at various developmental stages of *A. truncatum* seeds to gain insights into lipid biosynthesis and accumulation pathways. We explored candidate gene expression profiles during lipid metabolism, providing a foundation for further elucidation of lipid metabolism mechanisms and enhancing our understanding of the regulation of oil metabolism in *A. truncatum*.

2 Materials and Methods

2.1 Plant Materials Preparation

From May to October 2023, samara development of *A. truncatum* was monitored from anthesis to physiological maturity. Samples were collected in Pingdi Township, Panzhou City, Guizhou Province, China at two defined developmental stages. After collection, samaras were dissected, and the pericarp was removed with tweezers and a dissecting needle to expose the kernel. At physiological maturity, the seed coat is brown and the kernel is bright yellow. Developmental stages were defined by days after anthesis (DAA) together with external seed traits. Kernels at 150 DAA were designated as the immature stage (IMS),

and kernels at 180 DAA as the mature stage (MS). Three biological replicates were collected at each stage (n = 3), for a total of six samples: Y1-1, Y1-2, and Y1-3 (IMS) and Y2-1, Y2-2, and Y2-3 (MS). Excised kernels were snap-frozen in liquid nitrogen and stored at −80°C for fatty acid analysis and RNA extraction.

2.2 Oil Extraction and Lipid Analysis

Total lipids were extracted from seed samples using a chloroform–methanol mixture (1:1, v/v), following the lipid profiling protocol established by Shui et al. [26]. Triacylglycerols (TAGs) and diacylglycerols (DAGs) were quantified using an Exion UPLC–QTRAP 6500 PLUS system (Sciex), which was equipped with an electrospray ionization (ESI) source. The operating conditions included a curtain gas flow of 20, an ion spray voltage of 5500 V, a source temperature of 400°C, and ion source gases 1 and 2 both set at 35. Neutral lipids were isolated through isocratic elution on a Phenomenex Kinetex C18 column (2.6 μm, 4.6 × 100 mm) using a chloroform–methanol–0.1 mol L^{-1} ammonium acetate mixture (100:100:4, v/v/v) at a flow rate of 160 μL min^{-1} for 20 min. The quantification of individual TAG and DAG molecular species was performed using neutral loss MS/MS, employing a series of deuterium-labelled internal standards, including d5-TAG $(16:0)_3$, d5-TAG $(14:0)_3$, d5-TAG $(18:0)_3$, d5-DAG (1,3-16:0), and d5-DAG (1,3-18:1).

2.3 Lipidomics Data Processing and Statistical Analysis

Raw peak areas were normalized to the corresponding deuterium-labelled internal standards. Prior to multivariate analysis, lipid abundances were log10-transformed and Pareto-scaled. Unsupervised principal component analysis (PCA) was first used to evaluate sample clustering and detect outliers. Supervised orthogonal partial least squares-discriminant analysis (OPLS-DA) was then applied to assess group separation [27].

To reduce the risk of model overfitting, the OPLS-DA model was evaluated using cross-validation and permutation testing (n = 200 permutations). Model goodness-of-fit and predictability were reported as R2 and Q2, and the permutation-derived regression intercepts were used to judge whether the supervised model was robust. Differential lipids between developmental stages were determined by combining multivariate and univariate statistics. For each lipid, a two-sided Student's *t*-test was performed, and *p*-values were adjusted for multiple testing using the Benjamini–Hochberg false discovery rate (FDR). Lipids with VIP > 1.0, |log2(fold change)| > 1, and FDR-adjusted $p < 0.05$ were defined as significantly differential [28].

2.4 RNA Isolation, cDNA Library Construction, and RNA Sequencing

Total RNA was isolated from each seed sample using the mirVana miRNA Isolation Kit (Ambion, Foster City, CA, USA), adhering to the manufacturer's protocol. The quality of the RNA was initially assessed using 1% agarose gels, and the integrity of the samples was subsequently verified with an Agilent 2100 Bioanalyzer (Agilent Technologies, Santa Clara, CA, USA). For each library, 1.5 μg of high-quality RNA served as the starting material. Poly(A)+ mRNA was isolated from total RNA using oligo(dT)-conjugated magnetic beads and was then fragmented in the presence of divalent cations at an elevated temperature. First-strand cDNA synthesis was performed using random hexamer primers and M-MuLV reverse transcriptase (RNase H–), followed by second-strand cDNA generation utilizing DNA polymerase I in conjunction with RNase H. The resulting double-stranded cDNA fragments underwent end-repair to generate blunt ends, were adenylated at the 3′ termini, and were subsequently ligated to Illumina sequencing adapters. Adapter-ligated products of approximately 250–300 bp were selected using the AMPure XP system and amplified by PCR to yield the final libraries. The indexed libraries were pooled, loaded onto a flow cell for cluster generation, and sequenced on an Illumina HiSeq platform to obtain paired-end reads.

2.5 Data Processing, Assembly and Annotation

Raw sequencing reads in FASTQ format were initially subjected to quality control using custom Perl scripts. Sequences containing adapter remnants, poly-N stretches, and low-quality reads were filtered out to obtain a set of high-quality clean reads. For each library, standard quality metrics, including Q20, Q30, GC content, and sequence duplication rate, were calculated [29]. The clean reads were subsequently assembled *de novo* using Trinity. Within each Trinity component, isoforms assigned to the same locus were clustered, and the longest transcript in each cluster was retained as the representative unigene [29]. Functional annotation of unigenes was performed by comparing their sequences against several public databases, including the NCBI non-redundant protein (Nr) and nucleotide (Nt) databases, Pfam, KOG/COG, Swiss-Prot, KEGG Orthology (KO), and Gene Ontology (GO). BLASTx searches were conducted with an E-value threshold of 1.0×10^{-5}, and the top hits were utilized to assign putative functions and metabolic pathway information to each unigene [29].

2.6 Differential Expression Analysis

Transcript abundance was estimated from cleaned reads mapped back to the Trinity assembly, generating raw expected counts and TPM values for each unigene. TPM/FPKM values were used only for expression visualization. Differential expression between the immature stage (IMS) and mature stage (MS) was performed on raw counts using edgeR (negative binomial model) with TMM normalization and a quasi-likelihood framework. *p*-values were adjusted using the Benjamini–Hochberg false discovery rate (FDR), and genes with FDR < 0.05 and |log2(fold change)| > 1 were defined as differentially expressed [30,31]. Global expression patterns of DEGs were summarized by hierarchical clustering. Global expression patterns of DEGs were summarized by hierarchical clustering. GO enrichment was conducted using GOseq to correct for gene-length bias, and KEGG pathway enrichment was assessed using KOBAS [32].

2.7 Differential Expression Analysis

To validate the RNA-seq results, ten differentially expressed unigenes were selected for quantitative RT-PCR analysis. Gene-specific primers were designed using the PrimerQuest Tool, and the resulting PCR products were sequenced to confirm amplicon specificity. For each sample, 1 μg of total RNA was treated with gDNA Eraser and subsequently reverse-transcribed into first-strand cDNA using the PrimeScript™ RT Reagent Kit (RR047A). Each qPCR reaction (20 μL) contained 10 μL of abm® EvaGreen qPCR MasterMix (no dye), 1 μL of cDNA template, 1 μL of forward primer, 1 μL of reverse primer, and 7 μL of double-distilled water. Three biological replicates were analyzed for each sample. The cycling protocol included an initial denaturation at 95°C for 10 min, followed by 40–45 cycles of denaturation at 94°C for 15 s and annealing/extension at 60°C for 1 min. Relative transcript levels were calculated using the $2^{-\Delta\Delta Ct}$ method based on the corresponding threshold cycle (Ct) values. The primer sequences used for qRT-PCR are listed in Table S1.

3 Results

3.1 LC-MS Analysis of Lipid Extracts in Acer truncatum Seeds

Lipid composition was profiled using liquid chromatography–mass spectrometry (LC–MS). To robustly detect shifts in lipid abundance and minimize false-positive and false-negative results, three independent pairwise comparisons between sample groups were conducted. Lipid species were annotated based on retention time and MS/MS spectra, referencing published data and the LIPID MAPS database (http://www.

lipidmaps.org/). A total of 100 lipid molecular species were identified, comprising 66 triacylglycerols (TAGs) and 34 diacylglycerols (DAGs). The score plot from the orthogonal partial least-squares discriminant analysis (OPLS-DA) demonstrated tight clustering of samples within groups and clear separation between groups, indicating effective discrimination of the lipid profiles (Fig. 1a). Cross-validation was employed to assess the robustness of the OPLS-DA model, further supporting the reliability of the group separation (Fig. 1b).

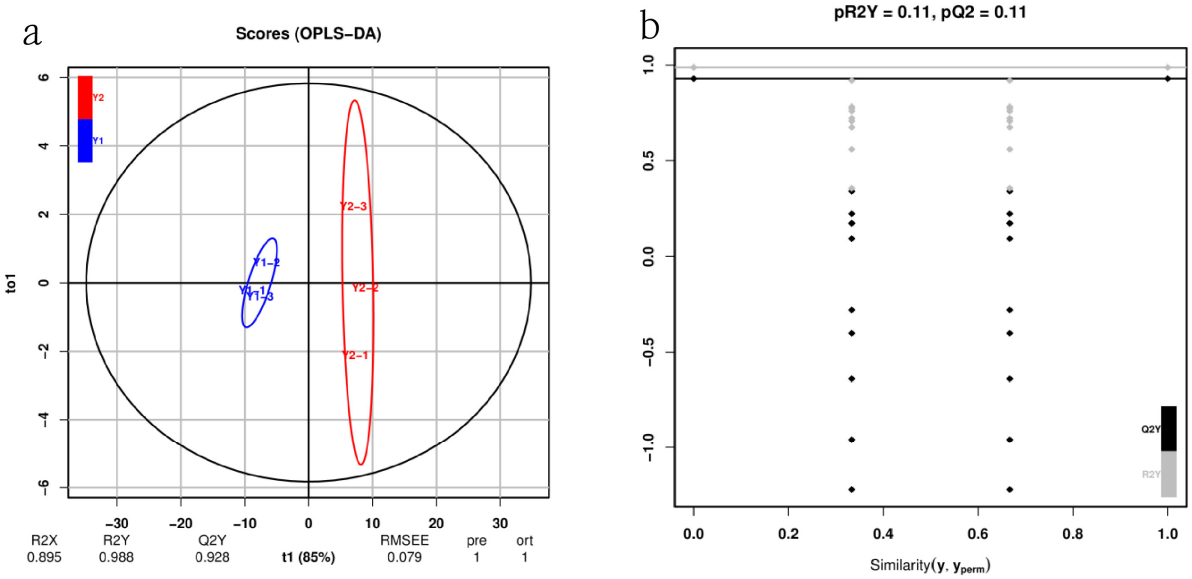

Figure 1: OPLS-DA models of Acer truncatum seeds. (**a**) OPLS-DA score plot of samples in MS and IMS. (**b**) Model validation by cross-validation and permutation testing (n = 200). R^2 indicates goodness-of-fit, whereas Q^2 assesses predictive ability. (**b**) Cross-validation plot The R^2 factor indicates a good fit, whereas the Q^2 coefficient assesses thepredictive power of the developed model by measuring the percentage of accurately classified samples through cross-validation. Two hundred permutations were conducted, and the resulting R^2 and Q^2 values were plotted.

3.2 The TAGs Content Increases in MS

Equations in display format should be separated from the surrounding text, aligned to the left of the cAs indicated by lipid-class-based clustering and heat maps, significant metabolic changes were observed among lipid species and in lipid composition (VIP > 1, $p < 0.05$) based on GC-MS analysis between the two stages (Fig. 2). In the mature stage (MS), the content of triacylglycerols (TAGs) increased markedly Compared to the immature stage (IMS), further confirming the pivotal role of TAGs in the accumulation of seed oil [13]. Most TAGs in the mature stage exhibited a significant increase relative to the immature stage. In contrast, the content of diacylglycerols (DAGs) showed minimal change, even demonstrating a slight downward trend. The lipid composition varies between the two stages, suggesting that there are different patterns of lipid metabolism in *A. truncatum* seeds during MS and IMS.

As illustrated in the heatmap, seed maturity did not significantly alter the abundance of various lipid species; however, the content of major triacylglycerol (TAG) species increased (Fig. 2). Further analysis using a volcano plot, with a threshold of p-value < 0.05 and |log2(fold change)| > 1 based on the Student's t-test, revealed 30 lipidomic metabolites (18 TAGs and 12 diacylglycerols, DAGs) exhibiting significant differential expression (Fig. 3d). The variations in the three most significant metabolites between mature seeds (MS) and immature seeds (IMS), namely TAG54:6 (18:1) (Fig. 3a), TAG54:5 (18:3) (Fig. 3b), and TAG54:6

(18:3) (Fig. 3c), are presented in the box plots. Notably, TAGs represented the majority of lipids in MS, accounting for over 91% of the total lipid content (Fig. 3e). Enhanced lipid accumulation of TAGs compared to DAGs was observed at both developmental stages.

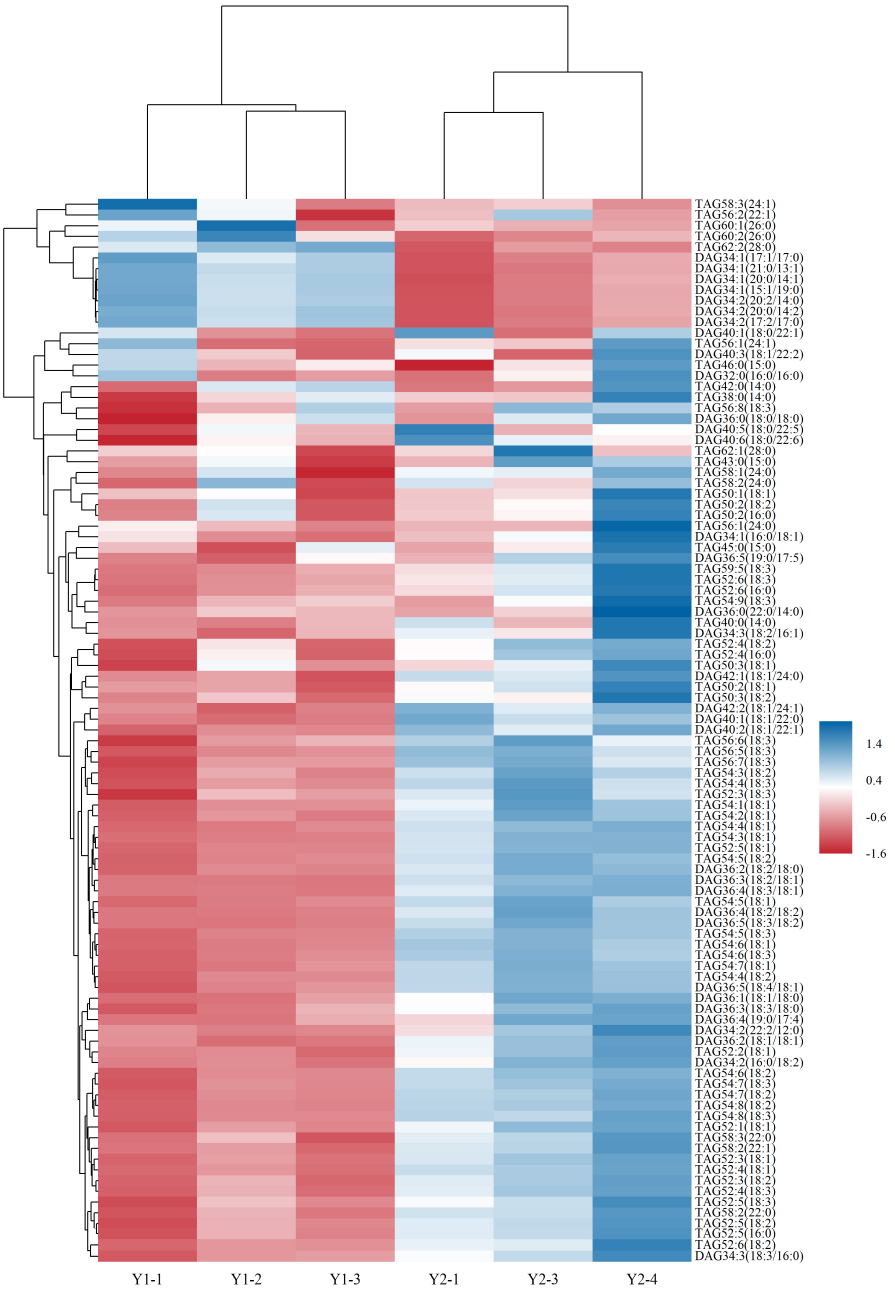

Figure 2: Heat map of samples in MS and IMS. Heat maps were applied to display the relative quantity of each lipid species, in which a gradient of red colors represents higher quantity while a gradient of blue colors represents lower quantity.

Lipidomics revealed complex specificity in glycerolipid remodeling during seed maturation. Compared with IMS, most triacylglycerols (TAGs) increased in MS (e.g., TAG54:3 and TAG54:5), whereas several TAG species decreased (e.g., TAG58:3). In parallel, many diacylglycerols (DAGs) showed lower relative abundance

in MS, consistent with DAG functioning as a central intermediate in plant glycerolipid metabolism that can be rapidly converted to TAG (via DGAT/PDAT) and interconverted with phosphatidylcholine during acyl editing. Together, we conclude that distinct metabolic patterns exist between MS and IMS, with lipid synthesis and accumulation primarily occurring in MS.

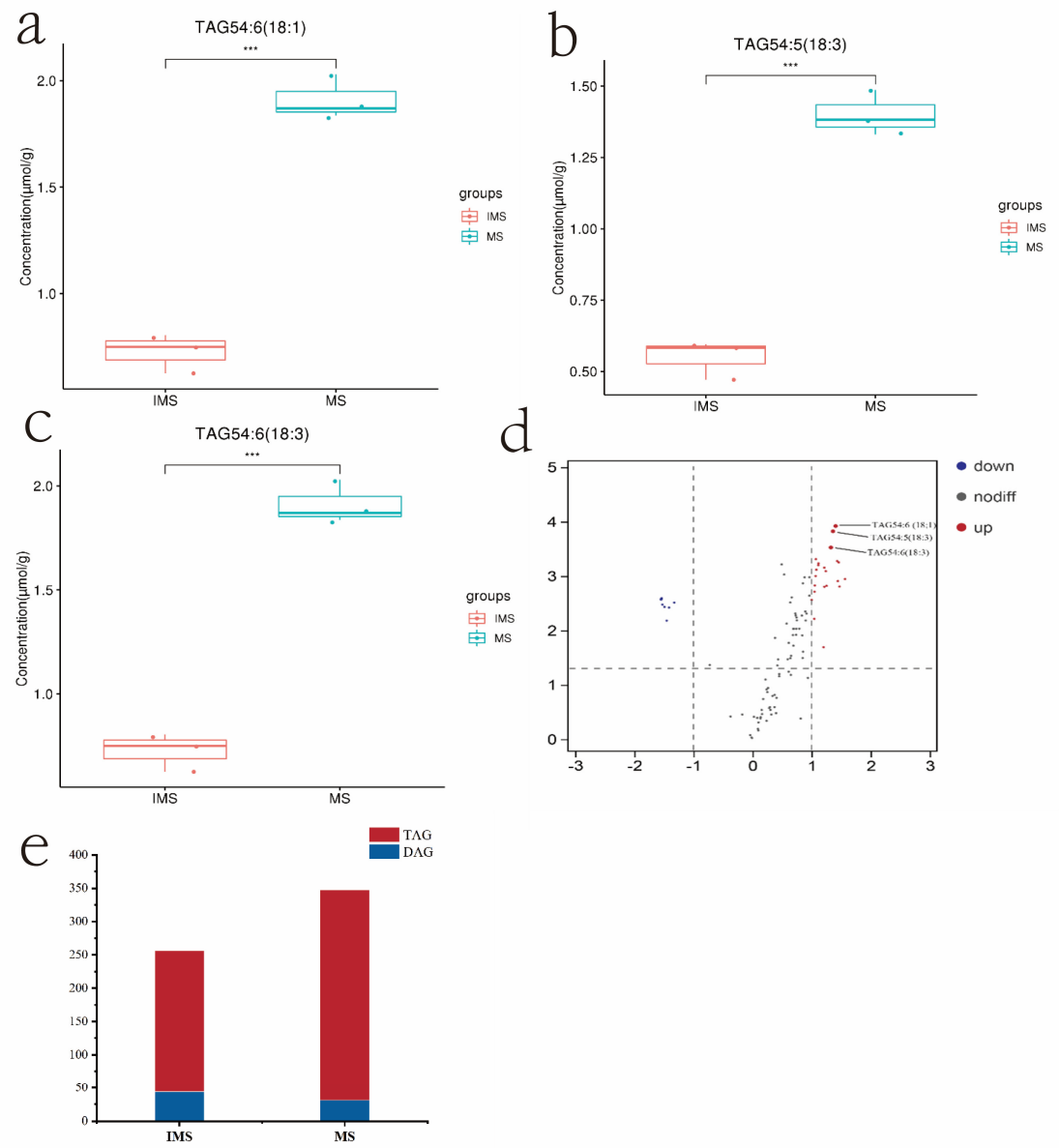

Figure 3: Changes in lipid composition during before and after *Acer truncatum* seeds maturity. (**a**–**c**) Box plots show the changes of the top 3 significant metabolites between MS and IMS. (***) indicate that there was *t* test *p* value < 0.001; df < 0.05. (**d**) Lipidomic metabolite (18 TAGs and 12 DAGs) with significant differential expression is depicted in the volcano plot. The *x* axis indicates that the significance changed, whereas the *y* axis indicates the fold change that was changed after the log10 transformation. Red points represent significantly differential expression lipidomic metabolites. The lipidomic metabolites that are not significantly different in expression are shown by the blue spots. (**e**) Proportions of TAGs and DAGs in the lipidomic metabolites in two stages. The proportions of TAGs are shown in the red columns, whereas the proportions of DAGs are indicated in the blue columns.

3.3 Transcriptome Sequencing and de novo Assembly

After quality filtering, we obtained 55,724,490, 48,095,836 and 57,736,034 clean reads from the immature-seed libraries (Y1-1, Y1-2 and Y1-3), and 47,965,770, 59,159,334 and 56,282,996 clean reads from the mature-seed libraries (Y2-1, Y2-2 and Y2-3). For each library, the yield of clean bases exceeded 7.19 Gb. As summarised in Table 1, the average sequencing error rate was 0.03%, the mean GC content was 46.32%, and the Q20 and Q30 values exceeded 97.50% and 93.03%, respectively, supporting the use of these data in subsequent analyses.

Clean reads were assembled *de novo* using Trinity into 56,225 unigenes. Unigene lengths ranged from 301 bp to 47,817 bp, with a median of 1339 bp and an N50 of 2338 bp. Of these, 19,949 unigenes were 200–500 bp, 15,337 were 500 bp–1 kb, 10,215 were 1–2 kb, and 10,724 exceeded 2 kb.

Table 1: Summary of transcriptome sequencing data.

Sample	Raw Reads	Clean Reads	Clean Bases	Error (%)	Q20 (%)	Q30 (%)	GC (%)
Y1-1	56,961,928	55,724,490	8.36 G	0.03	97.65	93.39	46.85
Y1-2	48,912,342	48,095,836	7.21 G	0.03	97.31	92.59	45.21
Y1-3	58,643,824	57,736,034	8.66 G	0.03	97.59	93.26	46.72
Y2-1	48,704,332	47,965,770	7.19 G	0.03	97.37	92.73	45.85
Y2-2	60,832,610	59,159,334	8.87 G	0.03	97.42	92.86	46.52
Y2-3	58,193,088	56,282,996	8.44 G	0.03	97.64	93.34	46.74
Average	55,374,687	54,160,743	8.12 G	0.03	97.5	93.03	46.32

3.4 Functional Annotation and Classification

The Nr, NT, Swiss-Prot, Pfam, KOG/COG, KEGG, GO databases were used to find all of the unigenes that were found. A total of 42,674 unigenes were annotated, representing 75.89% of the overall count. Among them, 5844 (10.39%) were annotated in all seven databases (Fig. 4a). A total of 11,161 unigenes (26.15%) demonstrated significant homology with sequences in the Nr database, with 13.3% matching *Citrus clementina* and 11.4% matching *Citrus sinensis* (see Additional file 1). Furthermore, the sequences from Fig. 4b showed that 7976 unigenes (18.9%) were substantially comparable to those in the KOG database.

According to GO annotation, 29,015 (67.99%) of the matched unigenes were classified into three functional categories: Biological Process, Cellular Component, and Molecular Function. As shown in the GO enrichment histogram, “cellular process” and “metabolic process” were the main subcategories in “Biological Process”. In the “Cellular Component” category, the subcategories “cell” and “cell part” showed the highest levels of enrichment. For “Molecular Function”, most unigenes were associated with “binding” and “catalytic activity” (Fig. 4c).

KEGG analysis, as a pathway-based approach, helps to better understand specific processes, gene functions, and gene interactions at the transcriptomic level. A total of 10,536 unigenes were mapped to 19 pathways, according to search results from the KEGG database. Unigenes from *A. truncatum* effectively represented pathways associated with lipid and carbohydrate metabolism (Fig. 4d).

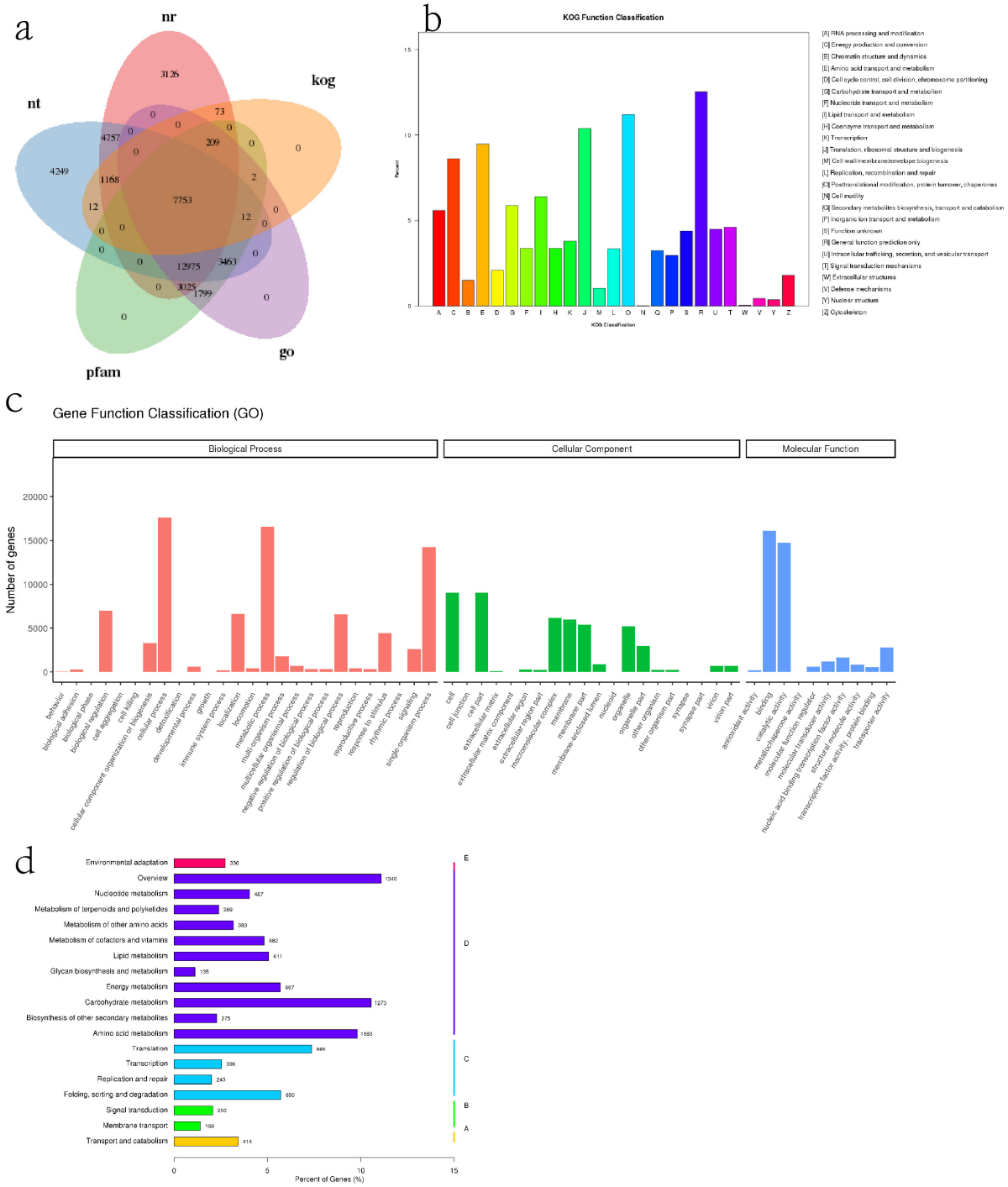

Figure 4: Gene functional annotation (**a**) Distribution of unigenes annotated by the top five databases. (**b**) Gene function classification annotated by Nr database. (**c**) Gene function classification annotated by GO database. (**d**) Gene function classification annotated by KEGG database.

3.5 Identification of Differentially Expressed Genes

Using the FPKM method, we calculated the expression of unigenes. Notably, we identified 3512 significant differentially expressed genes (DEGs) between the MS and IMS phases, with 2068 genes

upregulated (greater than 2-fold) and 1444 genes downregulated. The remaining genes exhibited downregulation (less than 0.5-fold). This finding suggests that lipid accumulation during seed maturity is accompanied by broad transcriptional reprogramming between these two stages. The proportion of expressed genes during the MS stage appears to increase in tandem with seed maturation (Fig. 5a). Hierarchical clustering analysis segregated the DEGs from the two stages into two distinct clusters. Genes in Cluster 1 were highly expressed in both the MS and IMS phases, whereas Cluster 2, which comprised the majority of the DEGs, exhibited contrasting expression profiles (Fig. 5b).

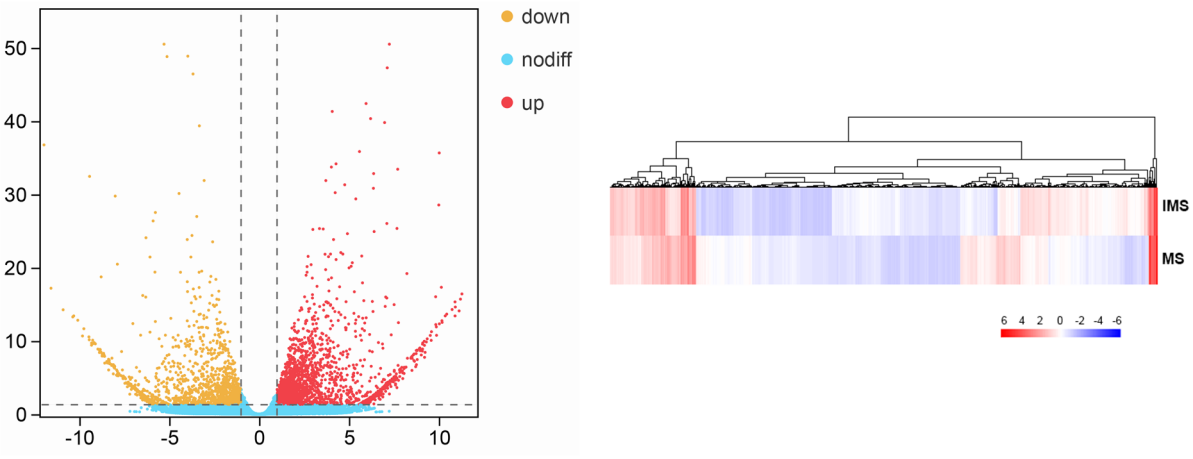

Figure 5: The pupation of *Acer truncatum* seeds induces the expression of genes involved in lipid metabolism. (**a**) The volcano plot illustrates the log2 fold changes in unigenes, where a fold change greater than 2 or less than 0.5 indicates a p-value of less than 0.05. The x-axis represents the −log10 transformed significance, while the y-axis represents the log2 transformed fold change. Red points denote up-regulated differentially expressed genes (DEGs), blue points indicate down-regulated DEGs, and grey points represent DEGs with insignificant changes. (**b**) The heatmap depicts the expression of unigenes at two developmental stages of *Acer truncatum* seeds, with a significance threshold of $p < 0.05$ and $\log2|FC| \geq 1$. The color gradient reflects the normalized expression values of unigenes, represented as log10 TPM, with red-highlighted genes exhibiting high expression levels and blue-highlighted genes showing low expression levels.

To further investigate the functional roles of the DEGs, 3512 genes were assigned to pathways in the KEGG database and to Gene Ontology (GO) categories. In the KEGG analysis, 219 DEGs were significantly enriched in 13 pathways (Fig. 6a). Among these, 202 upregulated genes were associated with 13 pathways, including “Biosynthesis of Unsaturated Fatty Acids”, “Fatty Acid Biosynthesis” and “Fatty Acid Elongation”, indicating a pronounced activation of lipid metabolic routes. In contrast, 17 downregulated genes were enriched in the “Phenylalanine, Tyrosine and Tryptophan Biosynthesis” pathway and in “Carotenoid Biosynthesis”.

GO enrichment analysis showed that, among the upregulated DEGs, 71 terms were assigned to biological processes, 266 to molecular functions and 434 to cellular components (Fig. 6b,c). For the 569 downregulated DEGs, 32 GO terms fell under biological processes, while 223 and 314 were grouped into molecular functions and cellular components, respectively. In both upregulated and downregulated gene sets, the term “metabolic process” was the most strongly enriched. Overall, genes involved in lipid metabolism tended to show higher transcript levels in the mature seed (MS) transcriptome than in the immature seed (IMS) transcriptome, consistent with an upregulation trend at the MS stage.

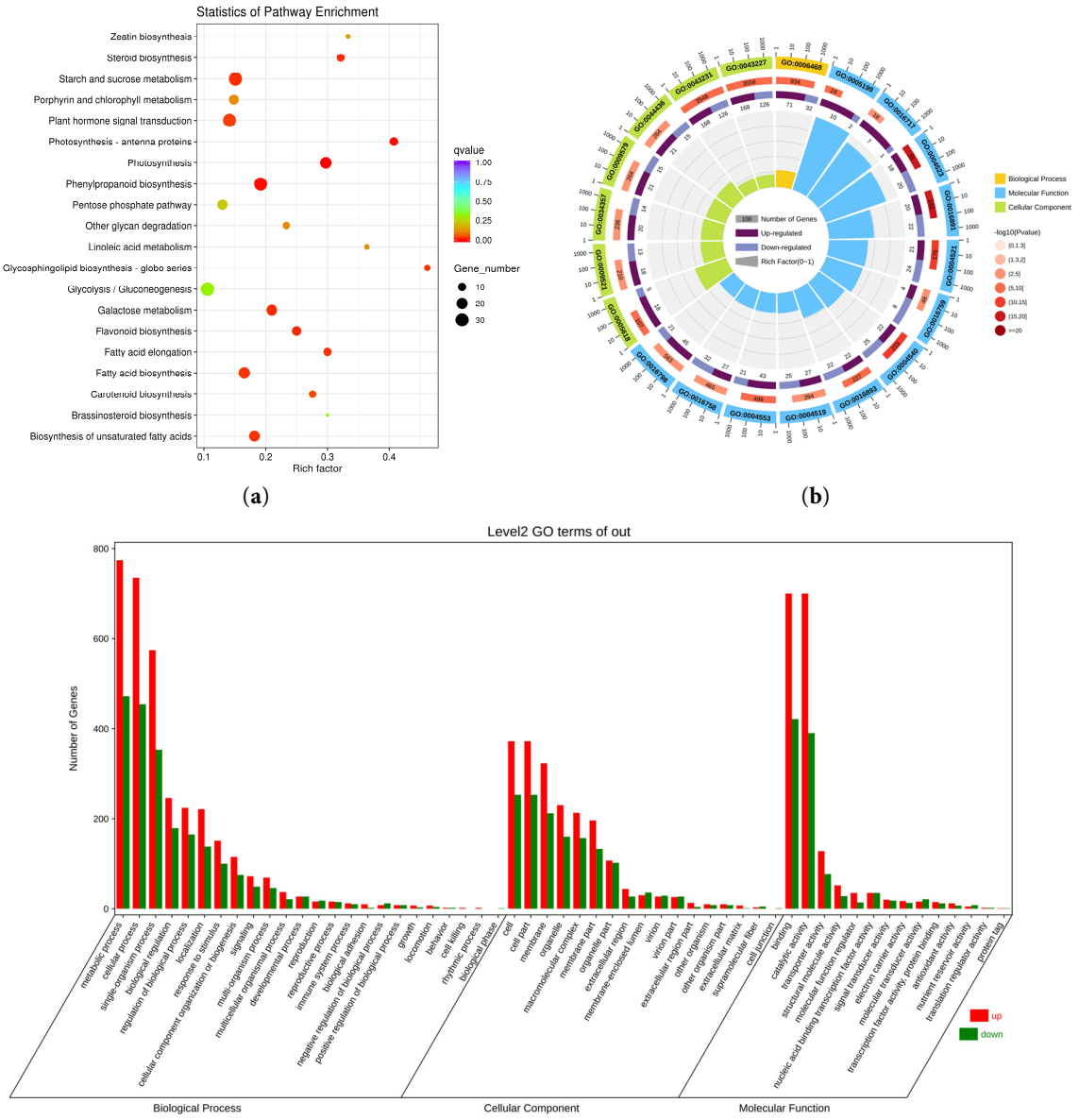

Figure 6: (**a**) The top 20 enriched pathways according to KEGG analysis of the total DEGs characterized in both IMS and MS. The size of the bubble indicates the input gene number in the pathway, and the color indicates the *p* value. The darker the color, the higher the degree of enrichment. (**b**) The GO enrichment circle diagram displays the GO terms enriched by differential genes. Each of the three major categories of GO (biological process, molecular function, cell composition) is represented by yellow, blue and green, and the related GO Term is displayed together through the inclusion relationship. The color depth represents the degree of enrichmen. (**c**) Classification of full-length transcripts in *Acer truncatum* seeds: the red columns represent upregulated GO classification and the green columns represent downregulated GO classification.

3.6 Quantitative RT-PCR Validation

The expression patterns of selected unigenes during two stages of *A. truncatum* seed maturation were determined by RT–qPCR for nine candidate genes. Nine genes were selected from differentially expressed

genes in enriched lipid-related pathways. Expression values for these genes are provided in Table S2. The expression patterns of the nine genes were consistent with the RNA-seq (FPKM) profiles (Fig. 7). Correlation analysis showed agreement between RT–qPCR and RNA-seq measurements (r > 0.815), supporting the consistency of the transcriptomic results.

AcDGAT (*diacylglycerol acyltransferase*) and *TER* (*trans-2,3-enoyl-CoA reductase*) showed lower expression in MS than in IMS, matching the reduced TAG biosynthesis at the MS stage. Gene-specific patterns were observed for *AcKCS* (*β-ketoacyl-CoA synthase*), *AcHACD* (*3-hydroxyacyl-CoA dehydratase*), and *AcKAR* (*β-ketoacyl-ACP reductase*). *AcHACD*, *KAR-2*, and *AcKCS-2* were higher in MS, whereas *AcHACD-2*, *AcKAR-1*, and *AcKCS-1* were lower in MS. *AcOLEOSIN* showed markedly higher expression in MS than in IMS.

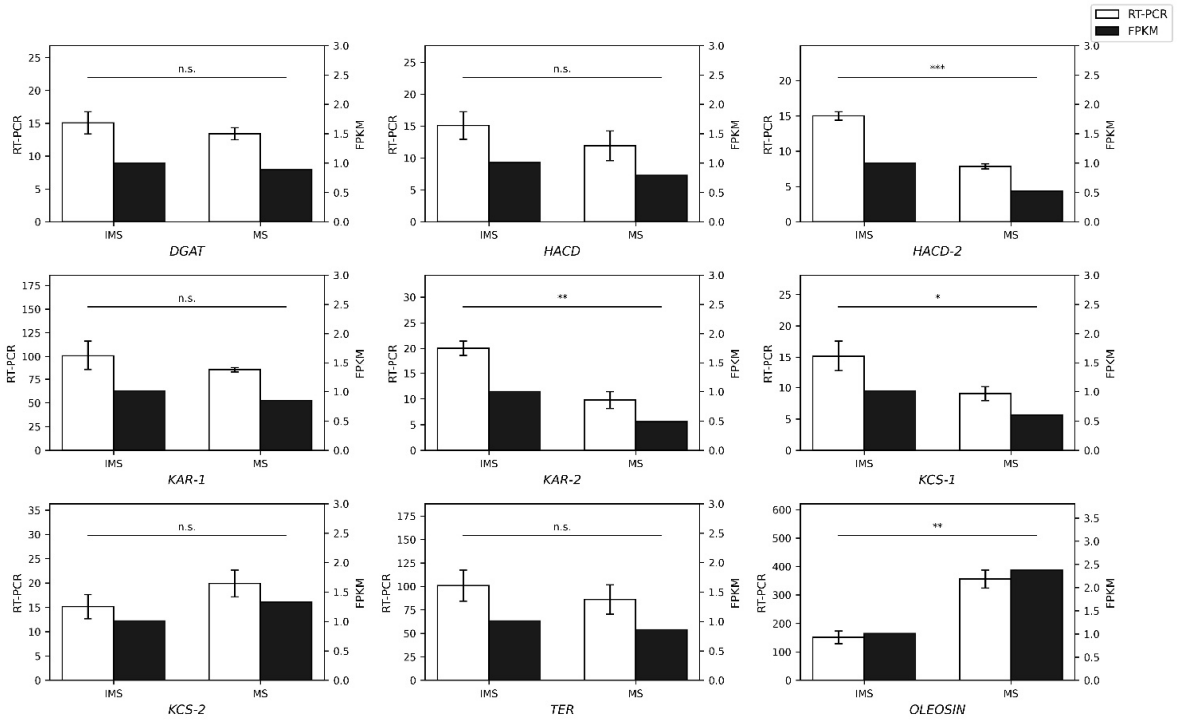

Figure 7: Comparison of RT-PCR and RNA-seq expression levels for nine selected genes between IMS and MS samples. For each gene (*DGAT, HACD, HACD-2, KAR-1, KAR-2, KCS-1, KCS-2, TER* and *OLEOSIN*), white bars represent RT-PCR expression levels (left *y*-axis) and black bars represent RNA-seq expression values expressed as FPKM (right *y*-axis) in IMS and MS, respectively. RT-PCR values are means ± SD of three biological replicates. Statistical significance of RT-PCR expression differences between IMS and MS was evaluated using a two-tailed Student's *t*-test; n.s., $^{*}p < 0.05$, $^{**}p < 0.0\ 1$, $^{***}p < 0.001$. n.s.: not significant.

3.7 Transcriptome and Metabolome Correlation Analysis

By linking transcript abundance with lipid composition through correlation analysis, we selected 12 unigenes. These unigenes encode enzymes or structural proteins implicated in fatty acid elongation and glycerolipid assembly and show pronounced, stage-associated expression shifts in the RNA-seq dataset. Annotation assigned these unigenes to *AcKCS*, *AcKAR*, *AcHACD*, *AcTER*, *AcDGAT*, *AcLPAT*, and *AcOLEOSIN*. Pearson correlation coefficients were calculated between unigene expression (FPKM) and the relative abundances of 30 quantified lipid metabolites (TAG and DAG molecular species) across two developmental stages. All 12 unigenes showed statistically significant correlations with the 30 lipid metabolites (Fig. 8).

Two *AcOLEOSIN* unigenes (*Cluster-16167.8397* and *Cluster-16167.12374*) were positively correlated with most TAG species, including multiple TAG54:x and TAG52:x species, and negatively correlated with several DAG species (e.g., DAG34:1, DAG34:2, and DAG34:4). The remaining 10 unigenes, annotated as *AcKAR*, *AcKCS*, *AcHACD*, *AcTER*, *AcDGAT*, and *AcLPAT*, showed the reverse association: positive correlations with DAG species and negative correlations with most TAG species.

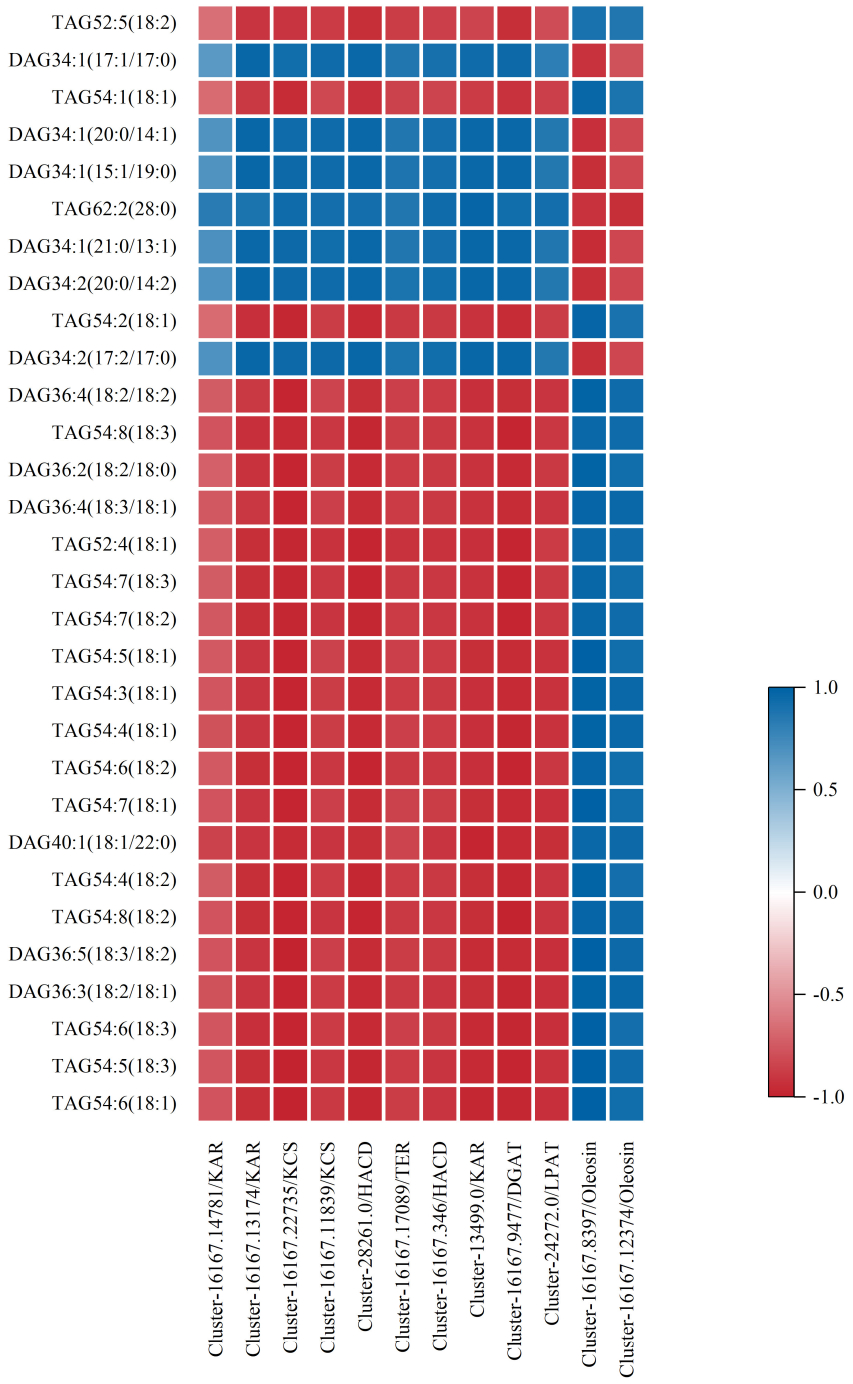

Figure 8: Heat map of the Pearson's correlation coefficient between gene expression level and intensity of lipid types in two stages.

4 Discussion

A. truncatum is a significant woody oil-bearing tree species and has been reported to contain various unsaturated fatty acids, including neuronic acid (NA) [10,25]. In seeds and fruits, Triacylglycerols (TAGs) represent a major renewable reservoir of reduced carbon used for food, industrial feedstocks, and biofuels production. The functional properties and economic value of plant oils are largely determined by the fatty acid (FA) composition of TAGs [12,33,34]. Diacylglycerols (DAGs) are glycerolipids containing two acyl chains and one free hydroxyl group, serving as key intermediates in glycerolipid metabolism that connect membrane-lipid remodeling with TAG assembly [35]; in the Kennedy pathway, DAG is acylated by DGAT to form TAG, and it can also be interconverted with phosphatidylcholine (PC) during acyl editing, thereby influencing the flux of acyl chains into storage lipids [35]. This study examined TAGs and DAGs metabolism during *A. truncatum* seed development, focusing on 150 days after anthesis (DAA) and 180 DAA, two stages associated with pronounced oil accumulation. Using gas chromatography–mass spectrometry (GC–MS), we identified and quantified 66 TAG species and 34 DAG species. TAGs accounted for more than 91% of total lipids in A. truncatum seeds, and TAG abundance exceeded DAG abundance at both stages. TAG content increased significantly at 180 DAA relative to 150 DAA, consistent with lipid deposition in oil bodies during seed maturation [36].

TAG and DAG concentrations varied across development, and these shifts corresponded to transcriptional changes in lipid-metabolism genes revealed by integrated lipidomics and transcriptomics analyses [35]. Mature seeds (MS) showed a marked increase in TAGs, whereas DAG levels remained relatively stable or declined, consistent with the metabolic routing of intermediates toward storage lipids during maturation [37]. Within the candidate genes highlighted by our dataset, *AcKCS* family members and *AcDGAT* are directly relevant to NA formation and TAG assembly. *AcKCS* participates in very-long-chain fatty-acid (VLCFA) elongation and is closely linked to NA biosynthesis, whereas DGAT catalyzes the terminal acylation step committing DAG to TAG [10,37]. At the same time, our RT-qPCR results indicate that *AcDGAT* transcript levels decrease at the MS stage while total TAG content rises sharply. This pattern suggests that TAG accumulation in late seed development is not explained by *AcDGAT* transcript abundance alone. Regulation beyond transcript level, isoform-specific contributions of different DGAT family members, and DGAT-independent routes such as PDAT-mediated acylation, as well as PC–DAG–TAG interconversion and acyl remodeling, may sustain TAG deposition as seeds mature. In addition, *AcOLEOSIN* homologs contribute to oil-body biogenesis and stability, and their expression often increases during the period of rapid TAG deposition. Taken together, our data support a model in which VLCFA elongation (KCS-related steps), TAG assembly through multiple enzymatic routes, and oil-body packaging jointly accompany the shift toward storage-lipid accumulation in mature *A. truncatum* seeds, rather than a model solely driven by DGAT transcription [38].

A. truncatum seed oil is rich in NA and other unsaturated fatty acids with nutritional and medicinal value. TAGs play metabolism also intersects with development and stress responses [39]. By characterizing TAG and DAG profiles during seed maturation and linking these traits to gene-expression patterns [39]. our results provide a molecular basis for improving oil yield and fatty-acid quality in this oilseed tree and expand current knowledge of lipid metabolism during seed development [11].

5 Conclusions

This study clarifies lipid metabolic pathways and associated regulatory features underlying seed-oil biosynthesis and accumulation in *A. truncatum*. TAGs were the predominant lipid class during seed maturation, with a significant increase relative to DAGs. Transcriptome analysis identified DEGs related

to lipid biosynthesis, including key enzyme genes such as *AcDGAT* and *AcKCS*, which displayed distinct expression patterns between immature and mature seeds. Integrated lipidome and transcriptome analyses indicate that seed lipid metabolism is tightly coordinated during development and highlight candidate genes and pathways linked to TAG accumulation. Comparison with functional evidence from homologous genes in other oil-bearing plants further supports the roles of KCS-mediated VLCFA elongation and DGAT-mediated TAG assembly, together with oil-body proteins such as OLEOSIN, in shaping TAG deposition during late seed development. These results provide a foundation for the genetic improvement of oil yield and fatty-acid quality in *A. truncatum*.

Acknowledgement: Not applicable.

Funding Statement: This work was supported by the Guizhou forestry project of Research and Demonstration Project on Key Technologies for Improving Quality and Efficiency of *Acer truncatum* Industry (Research 2022-18), National Natural Science Foundation of China (31860215, 32560369), and Guizhou Provincial Key Laboratory for Cultivation of Forest Trees in Plateau and Mountainous Areas (Qiaikehe Platform ZSYS [2025]025).

Author Contributions: Shengqun Chen: Conceptualization, Methodology, Formal analysis, Investigation, Writing—original draft. Lianwen Shen: Supervision, Investigation, Writing—review & editing. Shuang Qu: Formal analysis, Supervision, Investigation. Xia Jiang & Gang Wang: Conceptualization, Super vision, Project administration, Methodology, Writing—review & editing, Funding acquisition. All authors reviewed and approved the final version of the manuscript.

Availability of Data and Materials: The data that support the findings of this study are available from the corresponding author, Gang Wang, upon reasonable request.

Ethics Approval: Not applicable.

Conflicts of Interest: The authors declare no conflicts of interest.

Supplementary Materials: The supplementary material is available online at https://www.techscience.com/doi/10.32604/phyton.2026.078590/s1.

References

1. Gu RH, Morcol T, Liu B, Shi MJ, Kennelly EJ, Long CL. GC–MS, UPLC-QTOF-MS, and bioactivity characterization of *Acer truncatum* seeds. Ind Crops Prod. 2019;138:111480. [CrossRef].
2. Wang R, Liu P, Fan J, Li L. Comparative transcriptome analysis two genotypes of *Acer truncatum* Bunge seeds reveals candidate genes that influences seed VLCFAs accumulation. Sci Rep. 2018;8(1):15504. [CrossRef].
3. Fan Y, Lin F, Zhang R, Wang M, Gu R, Long C. *Acer truncatum* Bunge: a comprehensive review on ethnobotany, phytochemistry and pharmacology. J Ethnopharmacol. 2022;282:114572. [CrossRef].
4. Fan H, Sun L, Yang L, Zhou J, Yin P, Li K, et al. Assessment of the bioactive phenolic composition of *Acer truncatum* seed coat as a byproduct of seed oil. Ind Crops Prod. 2018;118:11–9. [CrossRef].
5. Song W, Zhang K, Xue T, Han J, Peng F, Ding C, et al. Cognitive improvement effect of nervonic acid and essential fatty acids on rats ingesting *Acer truncatum* Bunge seed oil revealed by lipidomics approach. Food Funct. 2022;13(5):2475–90. [CrossRef].
6. Ma Q, Wang Y, Li S, Wen J, Zhu L, Yan K, et al. Assembly and comparative analysis of the first complete mitochondrial genome of *Acer truncatum* Bunge: a woody oil-tree species producing nervonic acid. BMC Plant Biol. 2022;22(1):29. [CrossRef].
7. Li Q, Chen J, Yu X, Gao JM. A mini review of nervonic acid: source, production, and biological functions. Food Chem. 2019;301:125286. [CrossRef].
8. Liu F, Wang P, Xiong X, Zeng X, Zhang X, Wu G. A review of nervonic acid production in plants: prospects for the genetic engineering of high nervonic acid cultivars plants. Front Plant Sci. 2021;12:626625. [CrossRef].

9. Comlekcioglu N, Kutlu M. Fatty acids, bioactive substances, antioxidant and antimicrobial activity of *Ankyropetalum* spp., a novel source of nervonic acid. Grasas Aceites. 2021;72(1):e399. [CrossRef].
10. Yan L, Fang H, Liang Y, Wang Y, Ren F, Xie X, et al. Transcriptome analyses of *Acer truncatum* Bunge seeds to delineate the genes involved in fatty acid metabolism. BMC Genom. 2024;25(1):605. [CrossRef].
11. Li Y, Kong F, Wu S, Song W, Shao Y, Kang M, et al. Integrated analysis of metabolome, transcriptome, and bioclimatic factors of *Acer truncatum* seeds reveals key candidate genes related to unsaturated fatty acid biosynthesis, and potentially optimal production area. BMC Plant Biol. 2024;24(1):284. [CrossRef].
12. Xu C, Shanklin J. Triacylglycerol metabolism, function, and accumulation in plant vegetative tissues. Annu Rev Plant Biol. 2016;67:179–206. [CrossRef].
13. Bates PD, Stymne S, Ohlrogge J. Biochemical pathways in seed oil synthesis. Curr Opin Plant Biol. 2013;16(3):358–64. [CrossRef].
14. Bates PD, Browse J. The significance of different diacylgycerol synthesis pathways on plant oil composition and bioengineering. Front Plant Sci. 2012;3:147. [CrossRef].
15. Heil CS, Wehrheim SS, Paithankar KS, Grininger M. Fatty acid biosynthesis: chain-length regulation and control. Chembiochem. 2019;20(18):2298–321. [CrossRef].
16. Wan H, Liu H, Zhang J, Lyu Y, Li Z, He Y, et al. Lipidomic and transcriptomic analysis reveals reallocation of carbon flux from cuticular wax into plastid membrane lipids in a glossy "Newhall" navel orange mutant. Hortic Res. 2020;7:41. [CrossRef].
17. Yu SY, Zhang Y, Lyu YP, Yao ZJ, Hu YH. Lipidomic profiling of the developing kernel clarifies the lipid metabolism of *Paeonia ostii*. Sci Rep. 2021;11(1):12605. [CrossRef].
18. Cai WL, Yu SY, Hu YH. Synergistic mechanisms of DGAT and PDAT in shaping triacylglycerol diversity: evolutionary insights and metabolic engineering strategies. Front Plant Sci. 2025;16:1598815. [CrossRef].
19. Lin P, Wang K, Zhou C, Xie Y, Yao X, Yin H. Seed transcriptomics analysis in *Camellia oleifera* uncovers genes associated with oil content and fatty acid composition. Int J Mol Sci. 2018;19(1):118. [CrossRef].
20. Nakamura Y, Teo NZW, Shui G, Chua CHL, Cheong WF, Parameswaran S, et al. Transcriptomic and lipidomic profiles of glycerolipids during *Arabidopsis* flower development. New Phytol. 2014;203(1):310–22. [CrossRef].
21. Wei W, Wang LF, Tao JJ, Zhang WK, Chen SY, Song Q, et al. The comprehensive regulatory network in seed oil biosynthesis. J Integr Plant Biol. 2025;67(3):649–68. [CrossRef].
22. Liang Q, Wang W, Yuan F, Liu X, Li D, Yang KQ. Characterization of yuanbaofeng (*Acer truncatum* Bunge) samaras: oil, fatty acid, and phytosterol content. Ind Crops Prod. 2019;135:344–51. [CrossRef].
23. Qiao Q, Wang X, Ren H, An K, Feng Z, Cheng T, et al. Oil content and nervonic acid content of *Acer truncatum* seeds from 14 regions in China. Hortic Plant J. 2019;5(1):24–30. [CrossRef].
24. Wu Y, Yang Y, Liu C, Hou Y, Yang S, Wang L, et al. Potential suitable habitat of two economically important forest trees (*Acer truncatum* and *Xanthoceras sorbifolium*) in east Asia under current and future climate scenarios. Forests. 2021;12(9):1263. [CrossRef].
25. Ma Q, Sun T, Li S, Wen J, Zhu L, Yin T, et al. The *Acer truncatum* genome provides insights into nervonic acid biosynthesis. Plant J. 2020;104(3):662–78. [CrossRef].
26. Shui G, Guan XL, Low CP, Chua GH, Goh JSY, Yang H, et al. Toward one step analysis of cellular lipidomes using liquid chromatography coupled with mass spectrometry: application to *Saccharomyces cerevisiae* and *Schizosaccharomyces pombe* lipidomics. Mol Biosyst. 2010;6(6):1008–17. [CrossRef].
27. Pang Z, Lu Y, Zhou G, Hui F, Xu L, Viau C, et al. MetaboAnalyst 6.0: towards a unified platform for metabolomics data processing, analysis and interpretation. Nucleic Acids Res. 2024;52(W1):W398–406. [CrossRef].
28. Martínez S, Fernández-García M, Londoño-Osorio S, Barbas C, Gradillas A. Highly reliable LC-MS lipidomics database for efficient human plasma profiling based on NIST SRM 1950. J Lipid Res. 2024;65(11):100671. [CrossRef].
29. Yang Y, Xu M, Luo Q, Wang J, Li H. De novo transcriptome analysis of *Liriodendron chinense* petals and leaves by Illumina sequencing. Gene. 2014;534(2):155–62. [CrossRef].
30. Chen Y, Chen L, Lun ATL, Baldoni PL, Smyth GK. edgeR v4: powerful differential analysis of sequencing data with expanded functionality and improved support for small counts and larger datasets. Nucleic Acids Res. 2025;53(2):gkaf018. [CrossRef].
31. Raghavan V, Kraft L, Mesny F, Rigerte L. A simple guide to *de novo* transcriptome assembly and annotation. Brief Bioinform. 2022;23(2):bbab563. [CrossRef].

32. Bu D, Luo H, Huo P, Wang Z, Zhang S, He Z, et al. KOBAS-i: intelligent prioritization and exploratory visualization of biological functions for gene enrichment analysis. Nucleic Acids Res. 2021;49(W1):W317–25. [CrossRef].
33. Lu J, Xu Y, Wang J, Singer SD, Chen G. The role of triacylglycerol in plant stress response. Plants. 2020;9(4):472. [CrossRef].
34. Zhang Y, Gong H, Cui X, Gao C, Li N, Pu Y, et al. Integrated lipidomic and transcriptomic analyses reveal the mechanism of lipid biosynthesis and accumulation during seed development in sesame. Front Plant Sci. 2023;14:1211040. [CrossRef].
35. Hu W, Ma J, Zhang H, Miu X, Miao X, Deng Y. Integrated lipidomic and transcriptomic analysis reveals diacylglycerol accumulation in olive of Longnan (China). PeerJ. 2023;11:e15724. [CrossRef].
36. Gu J, Chao H, Wang H, Li Y, Li D, Xiang J, et al. Identification of the relationship between oil body morphology and oil content by microstructure comparison combining with QTL analysis in *Brassica napus*. Front Plant Sci. 2017;7:1989. [CrossRef].
37. Liu F, Yu S, Liu G. Mechanism and research progress of plant lipid regulation under biotie and abiotic stresses. Chin J Oil Crop Sci. 2023;45(5):1062–72. (In Chinese).
38. Bhatt-Wessel B, Jordan TW, Miller JH, Peng L. Role of DGAT enzymes in triacylglycerol metabolism. Arch Biochem Biophys. 2018;655:1–11. [CrossRef].
39. Yang Y, Benning C. Functions of triacylglycerols during plant development and stress. Curr Opin Biotechnol. 2018;49:191–8. [CrossRef].